Published in final edited form as:
Cell Rep. 2014 December 24; 9(6): 2018–2026. doi:10.1016/j.celrep.2014.11.036.

A Tethered Agonist within the Ectodomain Activates the Adhesion G Protein-coupled Receptors GPR126 and GPR133

Ines Liebscher[1,4,*,†], **Julia Schön**[1,†], **Sarah C. Petersen**[2], **Liane Fischer**[1], **Nina Auerbach**[1,2], **Lilian Marie Demberg**[1], **Amit Mogha**[2], **Maxi Cöster**[1], **Kay-Uwe Simon**[1], **Sven Rothemund**[3], **Kelly R. Monk**[2], and **Torsten Schöneberg**[1,*]

[1]Institute of Biochemistry, Medical Faculty, University of Leipzig, 04103 Leipzig, Germany

[2]Department of Developmental Biology, Washington University School of Medicine, St. Louis, MO 63110 USA

[3]Core Unit Peptide Technologies, Medical Faculty, University of Leipzig, 04103 Leipzig, Germany

[4]Novo Nordisk Center for Basic Metabolic Research, Department of Biomedical Sciences, University of Copenhagen, DK-2200 Copenhagen, Denmark

Abstract

Adhesion G protein-coupled receptors (aGPCRs) comprise the second largest yet least studied class of the GPCR superfamily. aGPCRs are involved in many developmental processes, immune and synaptic functions, but the mode of their signal transduction is unclear. Here, we show that a short peptide sequence (termed the *Stachel* sequence) within the ectodomain of two aGPCRs, GPR126 and GPR133, functions as a tethered agonist. Upon structural changes within the receptor ectodomain, this intramolecular agonist is exposed to the 7-transmembrane helix domain, which triggers G-protein activation. Our studies show high specificity of a given *Stachel* sequence for its receptor. Finally, the function of Gpr126 is abrogated in zebrafish with a mutated *Stachel* sequence, and signaling is restored in hypomorphic *gpr126* zebrafish mutants upon exogenous *Stachel* peptide application. These findings illuminate a previously unknown mode of aGPCR activation, and can initiate the development of specific ligands for this currently untargeted GPCR family.

[*]Correspondence to: T.S. (schoberg@medizin.uni-leipzig.de) or I.L. (liebscher@medizin.uni-leipzig.de).
[†]contributed equally to this work

I.L. and J.S. are joint first authors. I.L., J.S., L.F., K.-U.S., L.M.D. and T.S. performed the *in vitro* experiments. S.C.P., N.A., A.M. and K.R.M. performed and S.C.P. and N.A. analyzed the zebrafish experiments. I.L., J.S., L.F., T.S. analyzed the data. S.R. synthesized the peptides. I.L., T.S. designed the study and wrote the paper with contributions from all authors.

Introduction

Adhesion G protein-coupled receptors (aGPCRs) are among the largest proteins in nature and composed of a long extracellular domain (ECD), a seven-transmembrane domain (7TM) and an intracellular C-terminal tail (ICD) (Fig. 1A) (Bjarnadottir et al., 2004; McMillan et al., 2002). A further feature of the class is an autoproteolytic cleavage event that occurs at the GPCR Proteolytic Site (GPS), encompassed within the GPCR Autoproteolysis Inducing (GAIN) domain, which cleaves aGPCRs into an N-terminal fragment (NTF) and a C-terminal fragment (CTF) (Arac et al., 2012) (Fig. 1A). aGPCRs play essential roles in the control of cell and tissue polarity (Lawrence et al., 2007) and can modulate synaptic functions (O'Sullivan et al., 2012; Sudhof, 2001). Although increasing information about aGPCR relevance is available from mutant animal models, human diseases and variant-associated phenotypes, little is known about the molecular function, activation, and signal transduction of this receptor class (Langenhan et al., 2013; Liebscher et al., 2013).

The first indirect functional data for G-protein coupling by aGPCRs came from studies on GPR56 by knockdown experiments of $G_{12/13}$/p115 RhoGEF pathway components (Iguchi et al., 2008). An intriguing observation was reported in *gpr126* mutant zebrafish (zf), which exhibit defects in peripheral myelination (Monk et al., 2009). This phenotype was reversible through forskolin-induced cAMP elevation, suggesting G_s-protein coupling. More direct evidence for G_s-protein coupling was provided by measuring intracellular cAMP levels induced by basal activity of the aGPCRs GPR133 (Bohnekamp and Schoneberg, 2011) and GPR126 (Mogha et al., 2013). Further, experiments with chimeric G proteins, stoichiometric titrations of the $G\alpha_s$ subunit and the receptor as well as $G\alpha_s$ subunit knockdown experiments (Bohnekamp and Schoneberg, 2011) strongly support G-protein coupling for GPR133.

Although it is now clear that aGPCRs couple to G proteins, it remains unclear whether endogenous binding partners can induce activation of aGPCRs. Interestingly, increased aGPCR activity has been described for several aGPCRs when an N-terminal deletion mutant receptor is expressed (Okajima et al., 2010; Paavola et al., 2014; Paavola et al., 2011; Yang et al., 2011) (see Fig. 1A). These observations led to the assumption that the ectodomain functions as an inverse agonist, although at least two scenarios of aGPCR activation have been proposed (Liebscher et al., 2013): 1) the ectodomain contains an inverse agonist that inhibits 7TM signaling; 2) ligand binding at the ECD or NTF removal changes the conformation of an aGPCR and exposes a tethered agonist (suppl. Fig. S1A–B).

To test these two models, we used human (h) GPR126 and GPR133 to analyse the contribution of the ECD to receptor basal activity, since G_s-protein coupling has been experimentally suggested for these aGPCRs (Bohnekamp and Schoneberg, 2011; Gupte et al., 2012; Mogha et al., 2013). Systematic mutagenesis studies revealed tethered peptide sequences within the C-terminal-most part of the ECD that specifically activate G-protein signaling via 7TM interactions *in vitro*. Finally, we performed loss-of-function and rescue experiments in zf *gpr126* mutants to confirm the *in vivo* and evolutionarily conserved significance of the tethered agonist. Together, our study defines a previously unknown mechanism of aGPCR activation.

Results

ECD deletion activates GPR126 and GPR133

First, we deleted the ECDs of hGPR126 and hGPR133 at their natural GPS cleavage sites and tested the mutants in cAMP assays. In these constructs, termed CTF(GPR126) and CTF(GPR133), the NTF between the signal peptide and the GPS cleavage site was removed but the ECD part located C-terminally to the GPS cleavage site remained attached to the 7TM (CTF in Fig. 1B, suppl. Table S1). All mutants lacking the ECD displayed significantly increased basal activities in cAMP assays (Fig. 1C), consistent with results from other NTF-deficient aGPCRs. Both mutants were poorly detected at the cell surface via HA-tag staining (suppl. Fig. S1C). Accordingly, total ELISA and confocal imaging revealed an absence of the HA-tag in CTF(GPR126) constructs. However, confocal imaging of the C-terminal FLAG-tag showed specific membrane fluorescence (suppl. Fig. S1D). We therefore speculate that the HA tags in the CTF mutant constructs are processed during intracellular protein maturation, thereby precluding detection. Because the N termini of rhodopsin-like receptors can improve cell surface expression and detection of other GPCRs (Bohnekamp and Schoneberg, 2011; Staubert et al., 2010), we added an HA-tagged $P2Y_{12}$ N terminus to the residual ECD of the CTF mutants. This generated chimeric $P2Y_{12}$-CTF(GPR126) and $P2Y_{12}$-CTF(GPR133) receptors (Fig. 1B), which enabled proper plasma membrane detection via HA-tag visualization (suppl. Fig. S1C). As observed for the CTF constructs, $P2Y_{12}$-CTF(GPR126) and $P2Y_{12}$-CTF(GPR133) displayed high constitutive activity (Fig. 1C). These results demonstrate that deletion of the NTF activates hGPR126 and hGPR133.

The ECDs of GPR126 and GPR133 contain agonistic domains

We generated GPR126 and GPR133 mutants in which the entire ECD, including all of the GPS motif, was deleted or replaced by the N terminus of $P2Y_{12}$ (ΔGPS-CTF; $P2Y_{12}$-ΔGPS-CTF, Fig. 1B). None of the constructs displayed constitutive activity (Fig. 1C), although these chimeras were expressed at the cell surface (suppl. Fig. S1C). These results argue against the inverse agonist model of aGPCR activation because constitutive activity caused by release of an inverse agonist would not depend on the presence of the residual GPS motif. These results point towards an activation model that requires the residual GPS motif, and we hypothesized that the GPS sequence downstream of the cleavage site contains determinants required for receptor activation.

To identify this potential tethered agonist, we sequentially deleted amino acids (aa) C-terminal to the GPS cleavage site in GPR126. Functional analysis showed that while the N-terminal-most aa (Thr^{813}, Fig. 1B) was not essential for receptor activation (Fig. 1D), deletion of the first two as well as larger deletions that removed aa following Thr^{813} abolished basal receptor activity. This abolishment was not due to expression changes since total and cell surface expression levels were not significantly different between the constructs (suppl. Fig. S1E). To maintain correct aa length C-terminal to the cleavage site, we exchanged several positions with alanine. Again, mutants with an exchange of position 813 retained constitutive activity whereas the exchange of positions 815, 818 and 819 abolished activity in $P2Y_{12}$-CTF(GPR126) (Fig. 1E), while expression levels were not affected (suppl. Fig. S1F). Mutagenesis studies at corresponding positions in $P2Y_{12}$-

CTF(GPR133) revealed almost identical results (Fig. 1E; suppl. Fig. S1F). These experiments support the existence of a defined agonistic region C-terminal to the GPS.

A tethered peptide activates GPR126

To demonstrate that the aa sequence C-terminal to the GPS cleavage site has agonistic properties, we tested peptides derived from this domain on $P2Y_{12}$-ΔGPS-CTF(GPR126). Excitingly, systematic truncation of the peptide's C terminus revealed several agonistic peptides (Fig. 2A). The most efficient peptide, p16 (16 aa long), was used for further structure-function studies. N-terminal deletion of the first two aa abolished agonistic abilities of p16 (p16-1, p16-2; Fig. 2A). This does not contradict the results of Fig. 1D–E, because in the original CTF mutants, the first aa were replaced by the $P2Y_{12}$ N terminus or by alanine. Thus, these changes are tolerated, whereas the deletions in p16 are not. N-terminal extension beyond the cleavage site by 1 (p16+1) or 2–4 (p16+2 to p16+4) aa showed reduced and no agonistic activity of p16, respectively (Fig. 2A). This indicates that non-cleaved aa upstream of Thr^{813} are not part of the agonistic structure. In concentration-response curves, p16 displayed low potency (EC_{50} >400 μM) on both $P2Y_{12}$-ΔGPS-CTF(GPR126) and wild-type (wt) GPR126 (Fig. 2B), which can be explained by the natural 1:1 stoichiometry of the covalently bound agonist in its natural conformation. The higher cell surface expression of wt GPR126 compared to $P2Y_{12}$-ΔGPS-CTF(GPR126) (suppl. Fig. S1C) explains the increased efficacy of p16 on wt GPR126 activation. Time course analyses of cAMP accumulation (suppl. Fig. S2A) and GTPγS binding assays (suppl. Fig. S2B) in response to p16 were performed, supporting p16-induced G-protein coupling in GPR126-transfected cells. Note, eV transfected cells showed residual cAMP accumulation (Fig. 2C) and GTPγS binding, indicating endogenous expression of GPR126 in COS-7 cells. This was confirmed by RT-PCR (suppl. Fig. S2C), cAMP assays (Fig. 2C) and kinetic EPIC measurements with siRNA-mediated knockdown of the endogenous *GPR126* (suppl. Fig. S2D–E).

The endogenous expression of GPR126 and the high sensitivity of EPIC technology enabled us to test p16 apart from heterologous overexpression systems. As shown in Fig. 2D, p16 induced concentration-dependent cellular responses very similar to those found with isoprenaline and β-adrenergic receptor endogenously expressed in COS-7 cells. Mutation of position 6 ($Leu^{6}Ala$) in p16 abolished the response (Fig. 2D), confirming specificity. To identify functionally relevant positions in the peptide, we performed a systematic alanine scan (Fig. 2E). As expected from our receptor mutagenesis data (Fig. 1D/E), the more N-terminal aa (positions +2 to +7) are required for agonistic activity, whereas positions +8, +10, +12, and +14 to +16 can be replaced with Ala and still show agonistic properties. These data are in line with a high evolutionary conservation of the N-terminal portion of this peptide sequence (suppl. Fig. S2F). Interestingly, the peptide p16 $Gly^{4}Ala$ blocked p16-induced GPR126 activation at double concentration (Fig. 2F), indicating that p16 $Gly^{4}Ala$ can compete with the p16 binding site. Together, these data support the notion that the tethered peptide, p16, activates GPR126.

A tethered peptide activates GPR133

To determine if activation by a tethered peptide is common for aGPCRs, we performed similar studies with GPR133. The $P2Y_{12}$-ΔGPS-CTF(GPR133) can be activated by a peptide derived from the 13 aa (p13) downstream of the putative cleavage site (Fig. 3A). Concentration-response measurements of p13 revealed specific activity on $P2Y_{12}$-ΔGPS-CTF(GPR133) and wt receptor (EC_{50} >400 μM; Fig. 3B). The derived peptides were highly specific for the aGPCR from which they originated: GPR133 p13 did not activate GPR126, and GPR126 p16 did not activate GPR133 (Fig. 3C). Because the importance of GPS cleavage for aGPCR expression and activity has been controversially discussed (Liebscher et al., 2013), we tested two cleavage-deficient mutants, $GPR126T^{841}A$ (Moriguchi et al., 2004) and $GPR133H^{540}R$ (Bohnekamp and Schoneberg, 2011). Both mutants were expressed and activated by their respective peptides (suppl. Fig. S2G–I), indicating that cleavage at the GPS is not required for aGPCR activation by the tethered agonistic peptides. These data demonstrate that the tethered peptide, p13, activates GPR133. Together with our analysis of GPR126, these studies suggest that tethered peptide activation is a common signaling modality for the aGPCR class.

Tethered peptide activation of Gpr126 *in vivo*

We next sought to test the *in vivo* relevance of aGPCR tethered peptide activation. For these studies, we used zebrafish because previous mutant analyses demonstrated that Gpr126 is essential for Schwann cell myelination and ear development and that these physiological functions require cAMP elevation (Geng et al., 2013; Monk et al., 2009). Although several zf *gpr126* mutant alleles have been recovered in genetic screens (Pogoda et al., 2006), none specifically affect the tethered agonist sequence. Therefore, we utilized Transcription-Activator-Like-Effector-Nucleases (TALENs) to target this region (suppl. Fig. S3A–B); we isolated a mutant, $gpr126^{stl215}$, which lacks only two codons (Gly^{831}-Ile^{832}) within the tethered agonist sequence (Fig. 4A–B; suppl. Fig. S3C). $gpr126^{stl215}$ mutants were grossly normal compared to wt animals (suppl. Fig. S3D), but developed swollen ears (Fig. 4C), failed to express *myelin basic protein* (*mbp*, a marker of mature Schwann cells) along the posterior lateral line nerve (PLLn) (Fig. 4D–E) and did not myelinate peripheral axons (suppl. Fig. S3E–H). These defects completely phenocopy the previously published $gpr126^{st49}$ mutant, which has an early stop codon in the GAIN domain upstream of the GPS motif (Fig. 4B) (Monk et al., 2009). Importantly, the Gly^{831}-Ile^{832} deletion introduced by the $gpr126^{stl215}$ mutation does not alter cell surface expression of the receptor (suppl. Fig. S4A–B). We therefore conclude that the phenotypes observed in $gpr126^{stl215}$ mutants are caused by loss of a functional tethered agonist.

Finally, we tested whether p16 serves as an agonist for endogenous Gpr126 *in vivo* using zf PLLn *mbp* expression as an assay. The $gpr126^{st63}$ allele contains a point mutation in the first extracellular loop of the 7TM that converts a conserved cysteine residue to tyrosine ($C^{917}Y$, Fig. 4B) (Monk et al., 2009). This mutant receptor shows reduced cell surface expression compared to wt (~60% of wt levels; suppl. Fig. S4A) and a concomitant reduction in basal activity (suppl. Fig. S4B). *In vivo*, *mbp* expressed is reduced, but not absent, along the PLLn (Pogoda et al., 2006). In contrast, *mbp* expression is completely absent along the PLLn of the strong loss-of-function $gpr126^{st49}$ and $gpr126^{stl215}$ mutants (Fig. 4D–E). We therefore

predicted that the *gpr126*^{st63} allele produces a hypomorphic Gpr126 protein with reduced signaling capability. Accordingly, our ultrastructural analysis revealed that *gpr126*^{st63} mutants can myelinate axons in the PLLn, though fewer axons are myelinated than in wild-type (suppl. Fig. S4C–D) (Petersen et al., in revision).

Because we can infer that *gpr126*^{st63} mutants possess a partially functional 7TM, we hypothesized that exogenous addition of p16 could increase the signaling of endogenous hypomorphic Gpr126. This assay is feasible given that small molecules, including peptides, can freely diffuse into the developing larva in the presence of carrier (Morash et al., 2011) and because the functionally important positions in p16 are almost 100% identical between *D. rerio* and *H. sapiens* (suppl. Fig. S2F). Indeed, p16 was able to activate wt zf Gpr126 in *in vitro* cAMP assays (suppl. Fig. S4B). Therefore, we treated *gpr126*^{st63} mutants with 100 μM p16 in DMSO from 50–55 hours post-fertilization (hpf); this encompasses a temporal window in which cAMP elevation by forskolin administration can rescue myelination in *gpr126*^{st49} mutants (Glenn and Talbot, 2013; Monk et al., 2009). We then qualitatively scored *mbp* expression in the PLLn (Fig. 4A). As a negative control, we treated siblings with DMSO and observed normal PLLn *mbp* expression in wt (*gpr126*$^{+/+}$ or *gpr126*$^{st63/+}$) and reduced or absent *mbp* in hypomorphic *gpr126*$^{st63/st63}$ mutants (Fig. 4F–K). Treatment with 100 μM p16 caused no significant change in wt larvae but significantly rescued *mbp* expression in *gpr126*$^{st63/st63}$ hypomorphs (0% “strong” or “some” in *gpr126*$^{st63/st63}$ + DMSO vs. 44% “strong” or “some” in *gpr126*$^{st63/st63}$ + p16, Fig. 4H, J, K). To test whether this effect is specific to Gpr126 signaling, we also assayed strong loss-of-function *gpr126*^{st49} mutants, which presumably do not express a 7TM (Patra et al., 2013). Exogenous treatment of *gpr126*^{st49} mutants with 100 μM p16 did not rescue *mbp* expression in the PLLn (Fig. 4K), indicating that p16 signals through the 7TM. Together, the loss- and gain-of-function experiments in zebrafish demonstrate the *in vivo* relevance of tethered peptide activation of aGPCRs.

Discussion

We define a common intramolecular agonistic domain for the aGPCRs GPR126 and GPR133 that comprises a sequence between the GPS cleavage site and TM1. Because of its activating nature and its position at the very C terminus of the ECD, we refer to this agonistic sequence as the “*Stachel* sequence” (German word for “stinger”). Our analysis of *gpr126*^{stl215} suggests that *Stachel*-mediated activation of Gpr126 is essential for Schwann cell myelination in zebrafish (Fig. 4C–E; suppl. Fig. S3E–G); however, the *in vivo* mechanisms that unmask this tethered agonistic domain are unknown. GAIN domain crystal structures revealed that the *Stachel* sequence lies buried between two β-sheets (Arac et al., 2012). We and others have shown that CTF only truncation mutant aGPCRs possess increased basal activity (Fig. 1C–E) (Okajima et al., 2010; Paavola et al., 2014; Paavola et al., 2011; Yang et al., 2011); in all of these studies, the critical GAIN domain β-sheets are deleted along with the rest of the NTF, which presumably exposes the *Stachel* sequence. Therefore, structural changes *in vivo*, due to extracellular molecules interacting with the ECD (Langenhan et al., 2013; Liebscher et al., 2013) or even mechanical removal of the NTF may expose the *Stachel* sequence to activate the 7TM. The low affinity of the *Stachel*

sequence to the 7TM suggests a fast on-off ligand-receptor interaction and supports activation by mechanical signals (Karpus et al., 2013).

Peptide agonists usually bind to their cognate receptor in a sequential two-step mechanism (Monteclaro and Charo, 1996). The first step requires high affinity interactions with extracellular loop regions, whereas the second step is mediated by low affinity interactions with the helix bundle promoting receptor activation. Based on our findings, the first step is not required for aGPCRs, because the activating peptide is part of the receptor's own ECD and is therefore covalently bound to the 7TM. In the second step of our model of aGPCR activation, the *Stachel* sequence is predicted to interact with extracellular loops and upper helix bundles as in other peptide/peptide-GPCR pairs (Thompson et al., 2012) which requires a low affinity. This model is also consistent with protease-activated receptors in which thrombin cleaves the receptor's N terminus and exposes an activating tethered agonist (Vu et al., 1991).

Large ECDs are not unique to the aGPCR family. The ectodomains of glycoprotein hormone receptors (rhodopsin-like GPCR class) are also composed of several hundred aa forming leucine-rich repeat domains. In glycoprotein hormone receptors, a conserved module termed the hinge region (Sangkuhl et al., 2002) connects the ECD to the 7TM in a manner similar to the GPS domain in aGPCRs. Although the interspaced hinge region does not share predicted three-dimensional structural identity with the GPS motif, some features are similar. Namely, both the hinge region and the GPS motif possess multiple disulfide bonds forming at least two loops of the polypeptide chain (Arac et al., 2012). Interestingly, hinge region mutations of glycoprotein hormone receptors can activate these rhodopsin-like GPCRs, suggesting an "intramolecular agonistic unit" (Krause et al., 2012). Similarly, mutations in Cys^{775}, Cys^{794}, Cys^{807} and Cys^{809} of GPR126, which normally form disulfide bridges in the GAIN domain, displayed constitutive activity in cAMP assays (suppl. Fig. S4E–F). These data provide further evidence that structural changes in the GPS region promote activation via the Stachel sequence.

Our results are compatible with an activation scenario of aGPCRs in which an intramolecular agonistic domain (the Stachel sequence) is unmasked upon structural changes of the ECD, which subsequently triggers 7TM-mediated activation of G protein-signaling cascades (suppl. Fig. S1B, *cis* signaling; suppl. Fig. S4G). There is recent evidence that the ECD of GPR126 and of other aGPCRs can mediate biological functions independently of the 7TM (*trans* signaling) (Patra et al., 2013; Promel et al., 2012). Our discovery opens the possibility for further dissection between *trans*- and *cis*-dependent functions; for example, phenotypic perturbations in model organisms through peptide agonists can be attributed to the *cis*-signaling of the receptor (*e.g.*, Fig 4F–K). Our study defines a previously unknown signaling modality for aGPCRs, and can lay the foundation for rational ligand design that will promote deeper understanding of the physiology and therapeutic usefulness of this emerging class of GPCRs.

Experimental Procedures

aGPCR constructs and functional assays

Epitope-tagged full-length human aGPCR sequences were inserted into pcDps, and mutant aGPCRs were generated by PCR (suppl. Table S1). For functional assays, transfected COS-7 cells were split into 48-well plates and cAMP concentrations were determined with the Alpha Screen cAMP assay kit (PerkinElmer Life Sciences) according to the manufacturer's protocol. To measure label-free receptor activation, a dynamic mass redistribution (DMR) assay (Corning Epic Biosensor Measurements; Corning Life Sciences, Lowell, MA) with COS-7 cells endogenously expressing GPR126 was performed as described (Schroder et al., 2010). To estimate cell surface and total expression of receptors carrying N-terminal HA and C-terminal FLAG tags, ELISA was used (Schoneberg et al., 1998). Assay data was analyzed using GraphPad Prism version 6.0 for Windows (GraphPad Software, San Diego, CA) and statistical details are given in each figure legend.

Peptide synthesis

Solid phase peptide synthesis of the peptides was performed on an automated peptide synthesizer, MultiPep from Intavis AG (Köln, Germany), using standard Fmoc-chemistry.

Zebrafish studies

Adult zebrafish were maintained in the Washington University Zebrafish Consortium facility in accordance with institutional animal protocols (http://zebrafish.wustl.edu/husbandry.htm). Embryos were collected from heterozygous *gpr126* mutant adults and mutant larvae were compared to wild-type siblings for all assays. See suppl. methods for details on TALEN mutagenesis, *in situ* hybridization, transmission electron microscopy, and peptide treatment.

Additional methods

Additional details for all methods are available in suppl. Methods.

Supplementary Material

Refer to Web version on PubMed Central for supplementary material.

Acknowledgments

We thank Xianhua Piao and Thue W. Schwartz for their very helpful comments and discussion of the paper. We thank Marilyn Levy and Robyn Roth for assistance with TEM. The work was supported by the Deutsche Forschungsgemeinschaft (Sfb 610 to T.S.), the BMBF (IFB Adipositas Diseases Leipzig to J.S. and I.L.), NIH/NINDS (F32NS087786 to S.C.P. and R01NS079445 to K.R.M.), the Boehringer Ingelheim Fonds (MD stipend to N.A.) and the University Leipzig (Formel 1 start-up grant to I.L.).

The abbreviations used are

7TM	seven-transmembrane spanning domain
aa	Amino Acid

CTF	C-terminal fragment
ECD	extracellular domain
ELISA	enzyme-linked immunosorbent assay
eV	empty vector
GPCR	G protein-coupled receptors
GPS	GPCR proteolysis site
h	human
HA	hemagglutinin epitope
ICD	intracellular domain
mbp	myelin basic protein
NTF	N-terminal fragment
PLLn	posterior lateral line nerve
dpf	days post-fertilization
hpf	hours post-fertilization
SP	signal peptide
TM	transmembrane helix
wt	wildtype
WISH	whole mount *in situ* hybridization
zf	zebrafish

References

Arac D, Boucard AA, Bolliger MF, Nguyen J, Soltis SM, Sudhof TC, Brunger AT. A novel evolutionarily conserved domain of cell-adhesion GPCRs mediates autoproteolysis. Embo J. 2012; 31:1364–1378. [PubMed: 22333914]

Bjarnadottir TK, Fredriksson R, Hoglund PJ, Gloriam DE, Lagerstrom MC, Schioth HB. The human and mouse repertoire of the adhesion family of G-protein-coupled receptors. Genomics. 2004; 84:23–33. [PubMed: 15203201]

Bohnekamp J, Schoneberg T. Cell adhesion receptor GPR133 couples to Gs protein. J Biol Chem. 2011; 286:41912–41916. [PubMed: 22025619]

Geng FS, Abbas L, Baxendale S, Holdsworth CJ, Swanson AG, Slanchev K, Hammerschmidt M, Topczewski J, Whitfield TT. Semicircular canal morphogenesis in the zebrafish inner ear requires the function of gpr126 (lauscher), an adhesion class G protein-coupled receptor gene. Development. 2013; 140:4362–4374. [PubMed: 24067352]

Glenn TD, Talbot WS. Analysis of Gpr126 function defines distinct mechanisms controlling the initiation and maturation of myelin. Development. 2013; 140:3167–3175. [PubMed: 23804499]

Gupte J, Swaminath G, Danao J, Tian H, Li Y, Wu X. Signaling property study of adhesion G-protein-coupled receptors. FEBS Lett. 2012; 586:1214–1219. [PubMed: 22575658]

Iguchi T, Sakata K, Yoshizaki K, Tago K, Mizuno N, Itoh H. Orphan G protein-coupled receptor GPR56 regulates neural progenitor cell migration via a G alpha 12/13 and Rho pathway. J Biol Chem. 2008; 283:14469–14478. [PubMed: 18378689]

Karpus ON, Veninga H, Hoek RM, Flierman D, van Buul JD, Vandenakker CC, vanBavel E, Medof ME, van Lier RA, Reedquist KA, et al. Shear stress-dependent downregulation of the adhesion-G protein-coupled receptor CD97 on circulating leukocytes upon contact with its ligand CD55. J Immunol. 2013; 190:3740–3748. [PubMed: 23447688]

Krause G, Kreuchwig A, Kleinau G. Extended and structurally supported insights into extracellular hormone binding, signal transduction and organization of the thyrotropin receptor. PLoS One. 2012; 7:e52920. [PubMed: 23300822]

Langenhan T, Aust G, Hamann J. Sticky signaling--adhesion class G protein-coupled receptors take the stage. Sci Signal. 2013; 6:re3. [PubMed: 23695165]

Lawrence PA, Struhl G, Casal J. Planar cell polarity: one or two pathways? Nat Rev Genet. 2007; 8:555–563. [PubMed: 17563758]

Liebscher I, Schoneberg T, Promel S. Progress in demystification of adhesion G protein-coupled receptors. Biol Chem. 2013; 394:937–950. [PubMed: 23518449]

McMillan DR, Kayes-Wandover KM, Richardson JA, White PC. Very large G protein-coupled receptor-1, the largest known cell surface protein, is highly expressed in the developing central nervous system. J Biol Chem. 2002; 277:785–792. [PubMed: 11606593]

Mogha A, Benesh AE, Patra C, Engel FB, Schoneberg T, Liebscher I, Monk KR. Gpr126 functions in Schwann cells to control differentiation and myelination via G-protein activation. J Neurosci. 2013; 33:17976–17985. [PubMed: 24227709]

Monk KR, Naylor SG, Glenn TD, Mercurio S, Perlin JR, Dominguez C, Moens CB, Talbot WS. A G protein-coupled receptor is essential for Schwann cells to initiate myelination. Science. 2009; 325:1402–1405. [PubMed: 19745155]

Monteclaro FS, Charo IF. The amino-terminal extracellular domain of the MCP-1 receptor, but not the RANTES/MIP-1alpha receptor, confers chemokine selectivity. Evidence for a two-step mechanism for MCP-1 receptor activation. J Biol Chem. 1996; 271:19084–19092. [PubMed: 8702581]

Morash MG, Douglas SE, Robotham A, Ridley CM, Gallant JW, Soanes KH. The zebrafish embryo as a tool for screening and characterizing pleurocidin host-defense peptides as anti-cancer agents. Dis Model Mech. 2011; 4:622–633. [PubMed: 21729875]

Moriguchi T, Haraguchi K, Ueda N, Okada M, Furuya T, Akiyama T. DREG, a developmentally regulated G protein-coupled receptor containing two conserved proteolytic cleavage sites. Genes Cells. 2004; 9:549–560. [PubMed: 15189448]

O'Sullivan ML, de Wit J, Savas JN, Comoletti D, Otto-Hitt S, Yates JR 3rd, Ghosh A. FLRT proteins are endogenous latrophilin ligands and regulate excitatory synapse development. Neuron. 2012; 73:903–910. [PubMed: 22405201]

Okajima D, Kudo G, Yokota H. Brain-specific angiogenesis inhibitor 2 (BAI2) may be activated by proteolytic processing. J Recept Signal Transduct Res. 2010; 30:143–153. [PubMed: 20367554]

Paavola KJ, Sidik H, Zuchero JB, Eckart M, Talbot WS. Type IV collagen is an activating ligand for the adhesion G protein-coupled receptor GPR126. Sci Signal. 2014; 7:ra76. [PubMed: 25118328]

Paavola KJ, Stephenson JR, Ritter SL, Alter SP, Hall RA. The N terminus of the adhesion G protein-coupled receptor GPR56 controls receptor signaling activity. J Biol Chem. 2011; 286:28914–28921. [PubMed: 21708946]

Patra C, van Amerongen MJ, Ghosh S, Ricciardi F, Sajjad A, Novoyatleva T, Mogha A, Monk KR, Muhlfeld C, Engel FB. Organ-specific function of adhesion G protein-coupled receptor GPR126 is domain-dependent. Proc Natl Acad Sci U S A. 2013; 110:16898–16903. [PubMed: 24082093]

Pogoda HM, Sternheim N, Lyons DA, Diamond B, Hawkins TA, Woods IG, Bhatt DH, Franzini-Armstrong C, Dominguez C, Arana N, et al. A genetic screen identifies genes essential for development of myelinated axons in zebrafish. Dev Biol. 2006; 298:118–131. [PubMed: 16875686]

Promel S, Frickenhaus M, Hughes S, Mestek L, Staunton D, Woollard A, Vakonakis I, Schoneberg T, Schnabel R, Russ AP, et al. The GPS motif is a molecular switch for bimodal activities of adhesion class G protein-coupled receptors. Cell Rep. 2012; 2:321–331. [PubMed: 22938866]

Sangkuhl K, Schulz A, Schultz G, Schoneberg T. Structural requirements for mutational lutropin/choriogonadotropin receptor activation. J Biol Chem. 2002; 277:47748–47755. [PubMed: 12356766]

Schoneberg T, Schulz A, Biebermann H, Gruters A, Grimm T, Hubschmann K, Filler G, Gudermann T, Schultz G. V2 vasopressin receptor dysfunction in nephrogenic diabetes insipidus caused by different molecular mechanisms. Hum Mutat. 1998; 12:196–205. [PubMed: 9711877]

Schroder R, Janssen N, Schmidt J, Kebig A, Merten N, Hennen S, Muller A, Blattermann S, Mohr-Andra M, Zahn S, et al. Deconvolution of complex G protein-coupled receptor signaling in live cells using dynamic mass redistribution measurements. Nat Biotechnol. 2010; 28:943–949. [PubMed: 20711173]

Staubert C, Boselt I, Bohnekamp J, Rompler H, Enard W, Schoneberg T. Structural and functional evolution of the trace amine-associated receptors TAAR3, TAAR4 and TAAR5 in primates. PLoS One. 2010; 5:e11133. [PubMed: 20559446]

Sudhof TC. alpha-Latrotoxin and its receptors: neurexins and CIRL/latrophilins. Annu Rev Neurosci. 2001; 24:933–962. [PubMed: 11520923]

Thompson AA, Liu W, Chun E, Katritch V, Wu H, Vardy E, Huang XP, Trapella C, Guerrini R, Calo G, et al. Structure of the nociceptin/orphanin FQ receptor in complex with a peptide mimetic. Nature. 2012; 485:395–399. [PubMed: 22596163]

Vu TK, Hung DT, Wheaton VI, Coughlin SR. Molecular cloning of a functional thrombin receptor reveals a novel proteolytic mechanism of receptor activation. Cell. 1991; 64:1057–1068. [PubMed: 1672265]

Yang L, Chen G, Mohanty S, Scott G, Fazal F, Rahman A, Begum S, Hynes RO, Xu L. GPR56 Regulates VEGF production and angiogenesis during melanoma progression. Cancer Res. 2011; 71:5558–5568. [PubMed: 21724588]

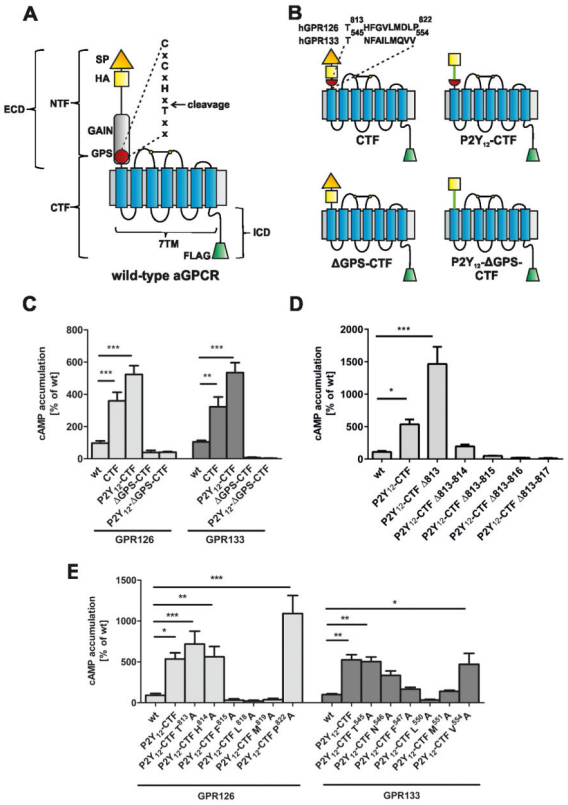

Fig. 1. Identification of a putative agonistic region in GPR126 and GPR133

(**A**) Cartoon of a prototypical aGPCR. The extracellular domain (ECD) contains a signal peptide (SP) and the GAIN/GPS domain. aGPCRs also possess a 7TM domain and an intracellular domain (ICD). Autoproteolysis at the GPS yields an N-terminal fragment (NTF) and a C-terminal fragment (CTF). For immunological detection, all constructs were epitope-tagged with an N-terminal HA epitope (yellow square) and a C-terminal FLAG epitope (green trapezoid). (**B**) hGPR126 and hGPR133 constructs, CTF and ΔGPS-CTF, were generated which lack the NTF and the ECD, respectively. Chimeric constructs were generated by fusing the N terminus of the human $P2Y_{12}$ receptor (green line) onto the GPR126 and GPR133 mutants. The red half-circle symbolizes the C-terminal portion of the GPS after its cleavage site. See also supp. Table S1. (**C–E**) cAMP levels from COS-7 cells transfected with wt and mutant GPR126 and GPR133. (**C**) $P2Y_{12}$-CTF mutants have increased basal activity compared to wt, which is abolished in ΔGPS-CTF mutants. (**D**) Constitutive activity of $P2Y_{12}$-CTF(GPR126) is increased by deletion of Thr^{813}. Receptor activity is abolished when the first three or more aa after the cleavage site are deleted. (**E**) Single positions within the C-terminal GPS sequence were mutated in GPR126 and GPR133 to alanine as shown. See suppl. Fig. S1C-F for expression studies of all constructs. Data are shown as means ± SEM of three independent experiments each performed in triplicates. EV served as negative control (eV; cAMP level: 3.68 ± 2.54 nM). Statistics were performed by two-way ANOVA and Bonferoni post-hoc test: *p<0.05; **p<0.01; ***p<0.001.

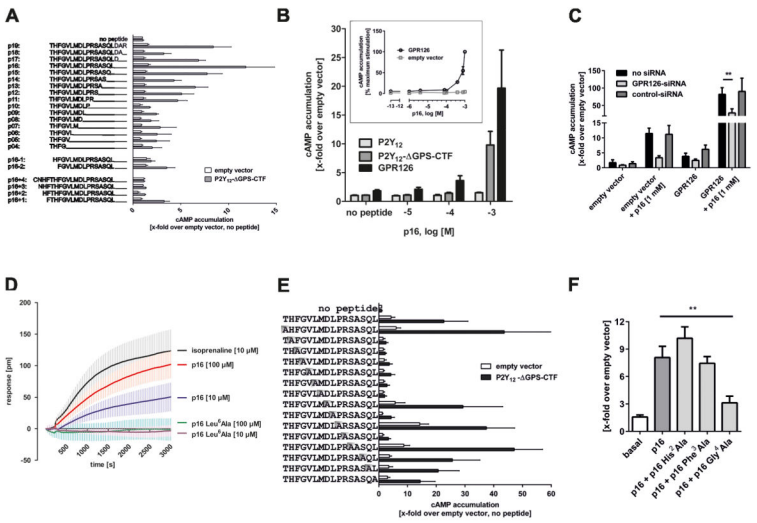

Fig. 2. GPR126 agonistic peptides are derived from the C-terminal part of the GPS

(**A**) Application of 1 mM peptides of different lengths derived from the C-terminal part of the GPS beginning at the cleavage site of GPR126 revealed agonistic properties as measured by cAMP accumulation. The highest agonistic efficacy was detected for a peptide containing 16 amino acids (p16). Negative controls: eV, and GPR126-$P2Y_{12}$-ΔGPS-CTF mutant. Basal cAMP levels were3.8 ± 1.6 nM. (**B**) Different p16 concentrations were tested on wt $P2Y_{12}$, wt GPR126, and $P2Y_{12}$-ΔGPS-CTF. Inset: concentration-response curve of p16 at wt GPR126 revealed an EC_{50} value >400 μM. Basal eV levels were 3.2 ± 0.7 nM. (**C**) COS-7 cells endogenously express low levels of GPR126 (see suppl. Fig S2C). Endogenous and transfected GPR126 are knocked down with primate GPR126-specific siRNA as shown by abolished cAMP formation (x-fold over eV; basal cAMP: 5.5 ± 2.2 nM). This was confirmed by a dynamic mass redistribution assay (Epic Biosensor Measurements) (suppl. Fig. S2D) and reduced cell surface ELISA (see suppl. Fig S2E). (**D**) The specificity of p16 was confirmed on endogenous GPR126. Mutation of position 6 (Leu^6Ala) abolished the response of p16 in EPIC measurements, as indicated by a picometer (pm) shift of the resonant wavelength caused by dynamic mass redistribution within the cell. (**E**) A systematic alanine-scan within the p16 peptide showed that the six amino acids downstream of Thr^{813} are required for receptor activation. Basal cAMP levels were 3.8 ± 1.6 nM. (**F**) p16 Gly^4Ala (1 mM) blocked activation of GPR126 by p16 (500 μM). Basal cAMP levels were 18.7 ± 9.4 nM. Data are shown as means ± SEM of three independent experiments each performed in triplicates. Statistics were performed by two-way ANOVA and Bonferoni post-hoc test: *p<0.05; **p<0.01; ***p<0.001.

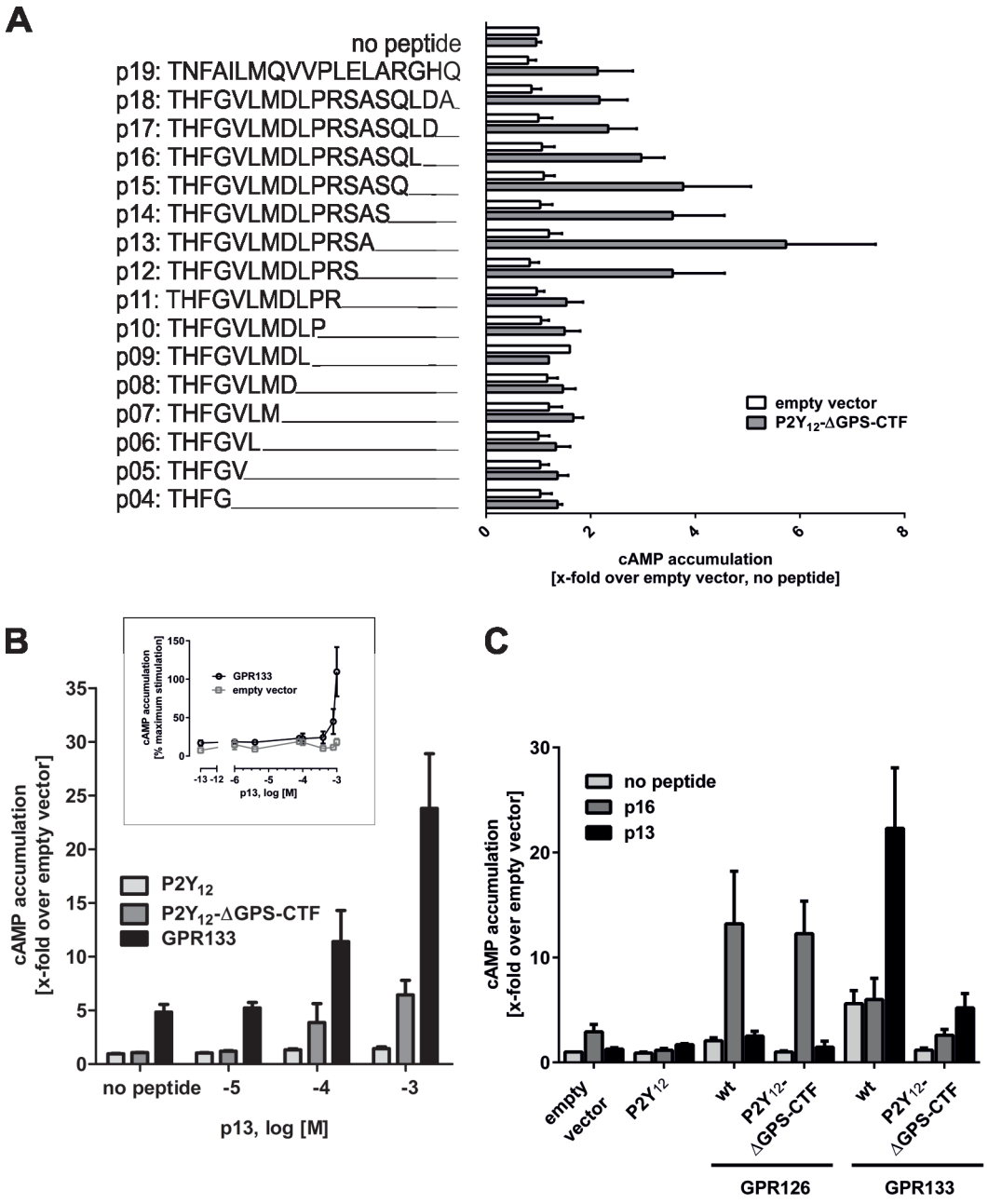

Fig. 3. Tethered agonistic peptides are receptor-specific

(**A**) Application of 1 mM peptides of different lengths derived from the C-terminal part of the GPS beginning at the cleavage site of GPR133 revealed agonistic properties as measured by cAMP accumulation. The highest agonistic efficacy was detected for a peptide containing 13 amino acids (p13). Negative controls: eV, and GPR126-$P2Y_{12}$-ΔGPS-CTF mutant. Basal cAMP levels were 5.2 ± 2.0 nM. (**B**) Concentration-response curve of the p13 peptide revealed an EC_{50} > 400 μM. Basal eV levels were 2.9 ± 0.2 nM. (**C**) Specificity of the p16 (GPR126) and the p13 (GPR133) peptides were verified using wt $P2Y_{12}$, wt GPR126 and wt GPR133 as controls. p16 peptide activated wt GPR126 and $P2Y_{12}$-ΔGPS-CTF(GPR126)

whereas it exhibited unspecific activity in control receptors due to endogenous expression of GPR126 in COS-7 cells (Fig. 2). The p13 peptide specifically activated wt GPR133 and $P2Y_{12}$-ΔGPS-CTF(GPR133). Basal cAMP levels were 3.0 ± 0.8 nM. Data are shown as means ± SEM of three independent experiments each performed in triplicates. Statistics were performed by two-way ANOVA and Bonferoni post-hoc test: *p<0.05; **p<0.01; ***p<0.001.

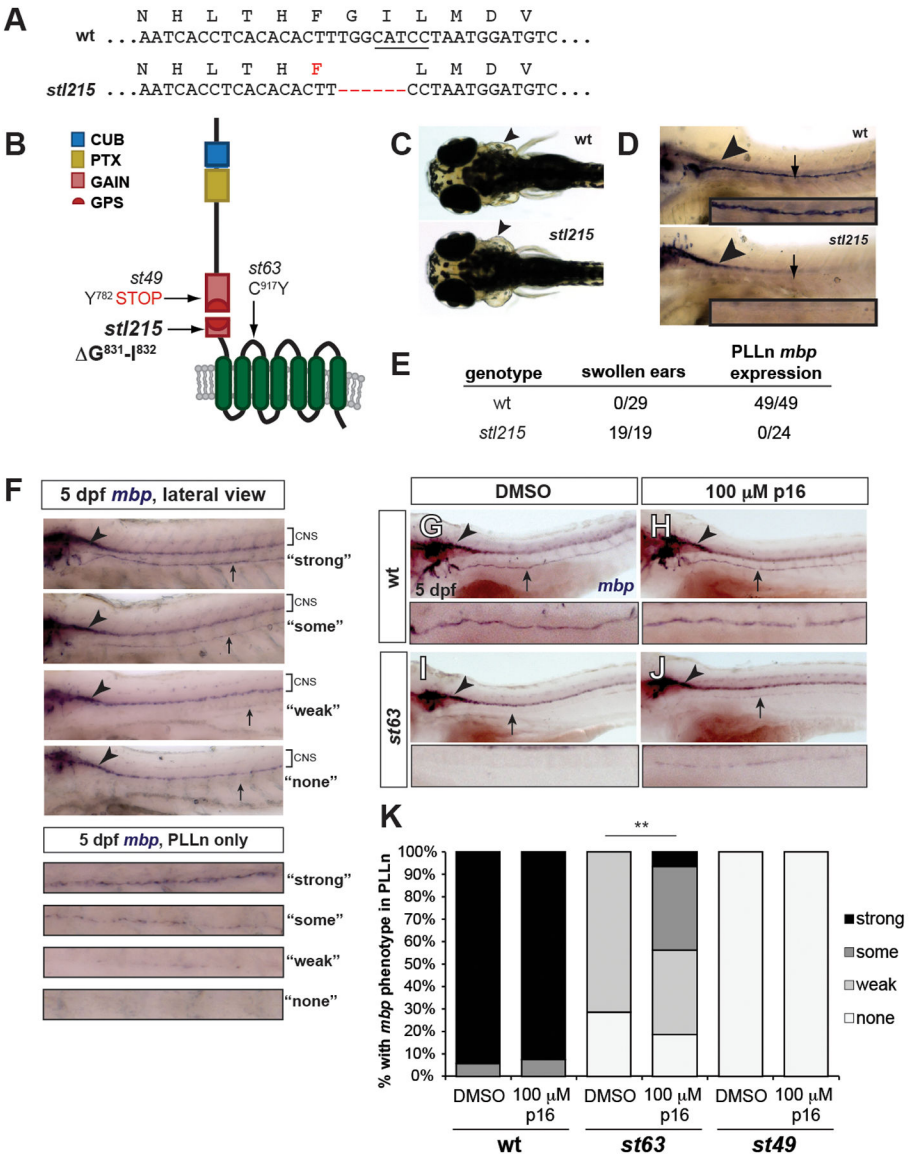

Fig. 4. Tethered agonistic peptides function *in vivo*

(**A**) Sequences of wild-type (wt) and *stl215* alleles. *stl215* is characterized by a 6 base pair (bp) in-frame deletion which results in the removal of amino acids Gly831 and Ile832. The BtsCI restriction enzyme site targeted by the TALEN is underlined. (**B**) Schematic representation of Gpr126 showing the *stl215* allele compared to *st49* and *st63* alleles. (**C**) Dorsal view of 4 dpf larvae. Arrowheads indicate normal ear morphology in the $gpr126^{+/+}$ larva (wt) and swollen ears in the $gpr126^{stl215/stl215}$ larva (*stl215*). (**D**) Lateral view of whole-mount *mbp in situ* hybridization (WISH) of zf larvae at 4 dpf. The posterior lateral line nerve (PLLn) is marked with an arrow; *mbp* expression in the central nervous system (CNS) is indicated with an arrowhead. *mbp* expression can be observed in the CNS but not in the PLLn of $gpr126^{stl215/215}$ mutant larvae (*st215*). **(E)** Quantification of swollen ear phenotype and PLLn *mbp* expression out of the total number of larvae scored per genotype (wt = $gpr126^{+/+}$ and $gpr126^{stl215/+}$). (**F–J**) WISH of 5 dpf larvae showing *mbp* expression

in CNS (arrowhead) and PLLn (arrow). (**F**) Scoring rubric for PLLn *mbp* expression, enlarged panels show PLLn only key. “Strong” = strong and consistent *mbp* expression, “some” = weak but consistent *mbp* expression, “weak” = weak and patchy *mbp* expression, “none” = no *mbp* expression. wt larvae treated with DMSO (**G**) or 100 μM p16 (**H**) have strong PLLn *mbp* expression. DMSO-treated *gpr126*$^{st63/st63}$ mutants have reduced PLLn *mbp* expression (**I**), which is significantly rescued with peptide treatment (**J**). (**K**) Quantification of WISH experiments. Bars indicate proportion of larvae with each PLLn *mbp* expression phenotype (as defined in **F**). **p<0.0001, combined *gpr126*$^{st63/st63}$ mutants with “some” and “strong” vs. combined *gpr126*$^{st63/st63}$ mutants with “weak” and “none”, Fisher’s Exact Test. wt = *gpr126*$^{+/+}$ and *gpr126*$^{+/st63}$ siblings of *gpr126*$^{st63/st63}$ mutants. N=3 technical replicates, n=105 wt (51 DMSO-treated, 54 peptide-treated), n=53 *gpr126*$^{st63/st63}$ (21 DMSO-treated, 32 peptide-treated), n=8 *gpr126*$^{st49/st49}$ (4 DMSO-treated, 4 peptide-treated).